Paper No.
2687

GALVANIC MODEL FOR LOCALIZED CO_2 CORROSION

Jiabin Han, Srdjan Nešić and Bruce N. Brown
Institute for Corrosion and Multiphase Technology
Department of Chemical and Biomolecular Engineering
Ohio University
342 West State Street, Athens, Ohio 45701

ABSTRACT

A galvanic model for localized CO_2 corrosion is proposed based on experimental evidence. The model has the capability to predict uniform corrosion on fresh and passive surfaces, and thus localized corrosion due to the galvanic cell establishment between them. Prediction of spontaneous passivation is at the core of this model. The model also has the potential to be extended to include a wide range of environmental factors, pit geometries and flow patterns. The model was experimentally validated at 80°C and pH 6.6. Numerical tests show that localized corrosion rates increase with increasing cathode/anode area ratio. In addition, pH and temperature influence localized corrosion propagation rates.

Key words: Model, corrosion, localized corrosion, spontaneous passivation, carbonic acid

INTRODUCTION

There are few valid mechanistic models of localized CO_2 corrosion. Schmitt developed a localized corrosion model based on the mechanism of flow induced localized corrosion (FILC) [1-7], where flow can fatigue the corrosion product films and then erode the substrate steel under violent "micro turbulence" within fractures. Achour qualitatively proposed a mechanistic model based on galvanic effects, hypothesizing that a galvanic cell could be established between the anodic pit surface and the film covered cathode. The open circuit potential difference between the anode and cathode of the cell was not experimentally quantified. The mathematical treatment for this galvanic effect had the open circuit potential of the cathode artificially set 100mV higher than that of the anode [8].

Previous research by J. Han and co-workers has revealed a localized CO_2 galvanic mechanism [9-11], depicted in Figure 1. Under scaling conditions, an iron carbonate film can be developed. Local conditions underneath the iron carbonate film facilitate formation of a passive film containing Fe_3O_4. This leads to a higher open circuit potential on the passivated surface than on the bare steel surface. When the intergrity of the films is corrupted, a galvanic cell can be established between the passivated surface and bare surface. This results in accelerated corrosion on the bared surface (anode) and retarded

corrosion on the passivated surface (cathode). The present electrochemical mechanistic model was developed to describe this physicochemical process. The key innovation of the current model is that it can predict the spontaneous passivation of the cathode as well as the galvanic potential difference and galvanic current in the established galvanic cell between bare pit surface (anode) and the passivated surrounding surface (cathode). Thus the polarized potential to the anode can be determined quantitatively.

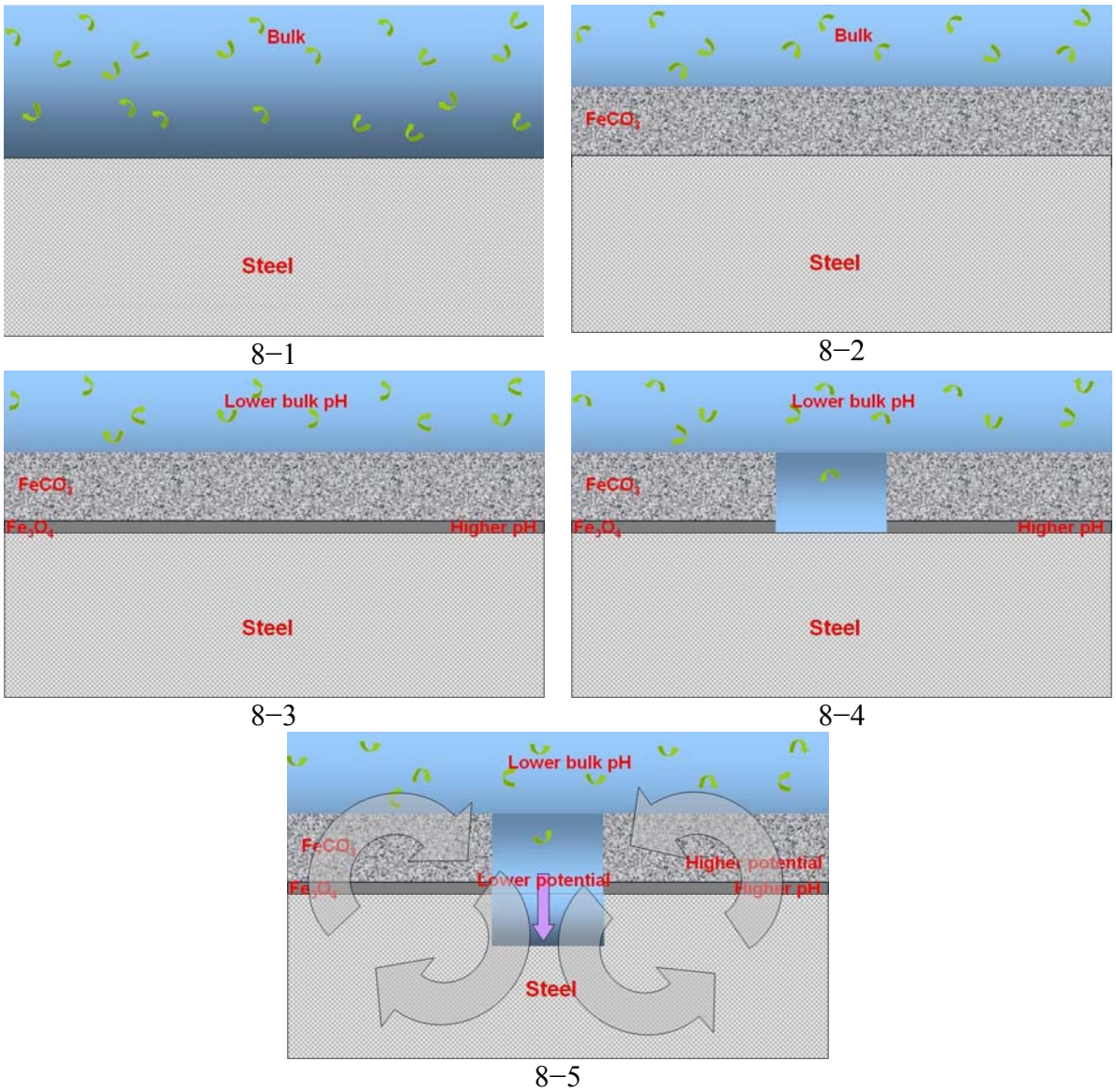

Figure 1 Scheme for 1-D galvanic mechanism of localized CO_2 corrosion on mild steel.

MODEL DESCRIPTION

The model describes a steady state "worst case" localized corrosion propagation scenario. The modeled galvanic cell is composed of an active anode and a completely passivated cathode.

The model is defined and constructed mainly by mathematically describing the water chemistry mass transfer and the electrochemical processes. The electrochemical part includes three models: the active corrosion model on the bare active surface, the spontaneous passivation model on the cathode surface and a localized galvanic cell model established between anode and cathode. The water

chemistry model describes all the chemical reactions in CO_2 aqueous environments, including CO_2 gas dissolution, CO_2 hydration, carbonic acid dissociation and water dissociation. The following text describes the model in detail.

Water Chemistry Model

The CO_2 in the gas phase dissolve in the aqueous solution and then hydrates to produce carbonic acid. This species partially dissociates in the solution to produce protons and bicarbonate ions. Bicarbonate ions further dissociate and generate carbonate ions and protons.

$$CO_{2(g)} \xleftrightarrow{K_{Henry,CO_2}} CO_{2(aq)} \tag{1}$$

$$CO_{2(aq)} + H_2O_{(aq)} \xleftrightarrow{K_{hyd}} H_2CO_{3(aq)} \tag{2}$$

$$H_2CO_{3(aq)} \xleftrightarrow{K_{ca}} H^+_{(aq)} + HCO^-_{3(aq)} \tag{3}$$

$$HCO^-_{3(aq)} \xleftrightarrow{K_{bi}} H^+_{(aq)} + CO^{2-}_{3(aq)} \tag{4}$$

$$H_2O_{(aq)} \xleftrightarrow{K_w} H^+_{(aq)} + OH^-_{(aq)} \tag{5}$$

More details related to these equilibria have been published previously [12-14] and will not be repeated here.

Electrochemistry Model

The electrochemistry model is composed of three modules to describe the active steel dissolution reactions at the anode, the spontaneous passivation reaction on the cathode and the galvanic cell establishment between the anode and the cathode.

Reactions on the anode: The overall anodic reaction on the anode is the iron dissolution:

$$Fe_{(s.)} \rightarrow Fe^{2+}{}_{(aq.)} + 2e^- \tag{6}$$

The cathodic reactions occurring on the anode are carbonic acid reduction, proton reduction and water reduction:

$$2H_2CO_{3(aq)} + 2e^- \rightarrow H_{2(g)} + 2HCO^-_{3(aq)} \tag{7}$$

$$2H^+{}_{(aq)} + 2e^- \rightarrow H_{2(g)} \tag{8}$$

$$2H_2O_{(aq)} + 2e^- \rightarrow H_{2(g)} + 2OH^-{}_{(aq)} \tag{9}$$

Both the anodic and cathodic reactions on the anode are schematically shown in Figure 2. In this mathematical model, the electrochemical parameters and physical properties used to describe these

electrochemical reactions were previously described by Nešić et al. [12-14] and will not be reproduced here.

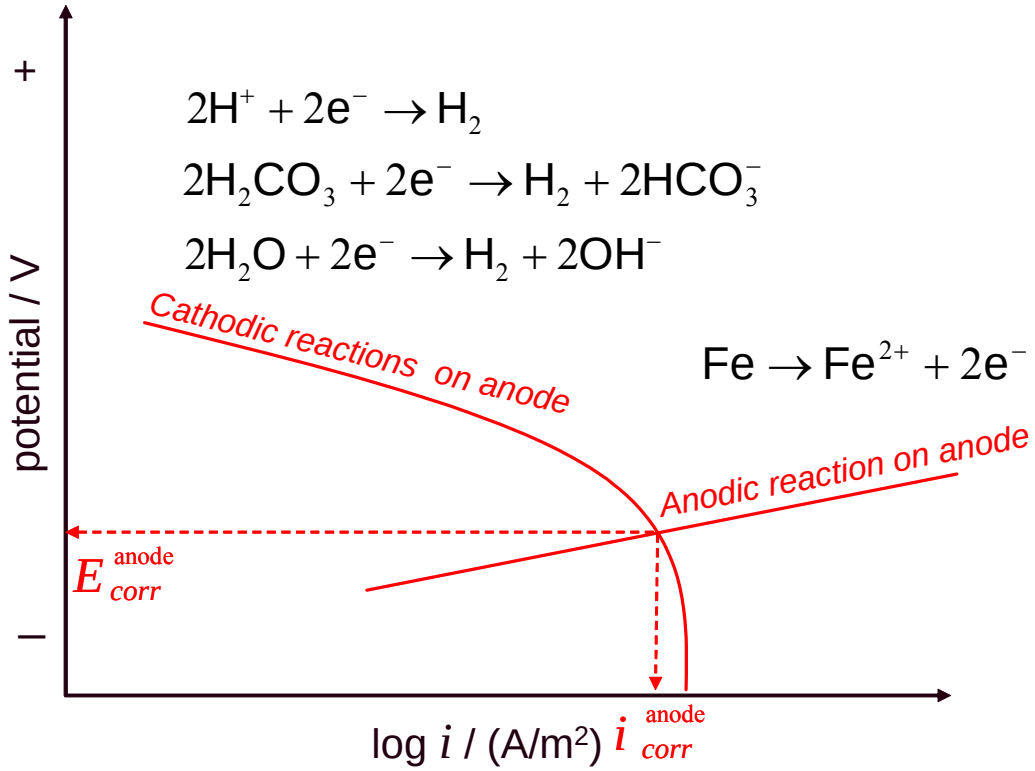

Figure 2 Schematic representation of active corrosion on the bare anode surface (pit bottom).

Modeling spontaneous passivation on the cathode: A passive film, which is likely a form of oxide such as Fe_3O_4 [11], can form beneath a protective iron carbonate film leading to passivation of the cathode [10]. The anodic reaction on the passivated cathode is passive dissolution of iron. The overall anodic reaction for the passive anodic dissolution of iron can be written as:

$$3Fe_{(s)} + 8OH^-_{(aq)} \rightarrow Fe_3O_{4(s)} + 8e^- + 4H_2O_{(aq)} \quad (10)$$

This corresponds to the vertical region of the anodic polarization curve in Figure 3:

The passivation current density, a kinetic parameter, describing the passive iron dissolution reaction on the cathode (Figure 3), has to be experimentally determined; little information on spontaneous passivation of mild steel has been reported in the literature. The passivation current density for the anodic reaction appears to be independent of pH as shown in Figure 4. These data were obtained from corrosion rate measurements after the achieving spontaneous passivation on the steel surface exposed to CO_2 aqueous environments.

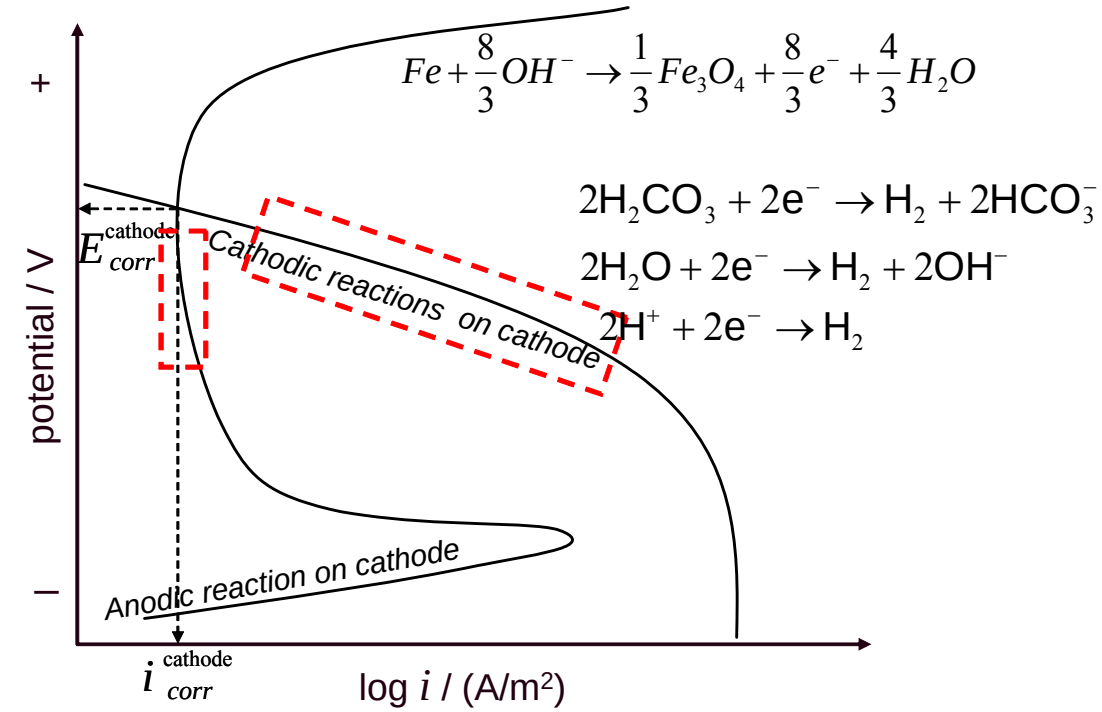

Figure 3 Schematic representation of passive corrosion on the cathode (iron carbonate covered steel surface around the pit).

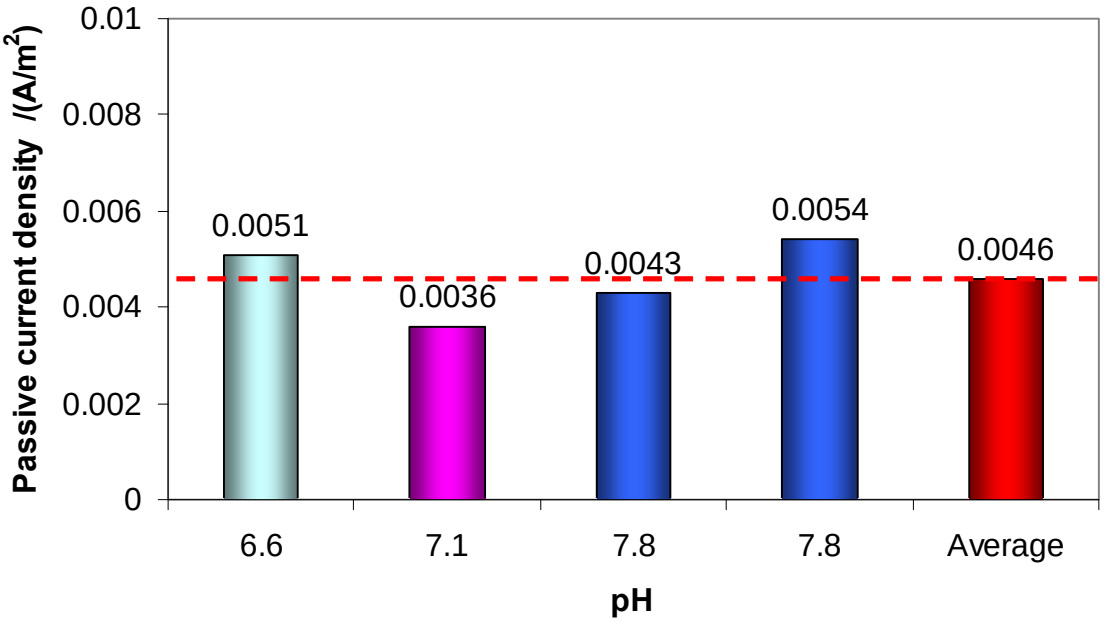

Figure 4 Spontaneous passivation current density as a function of pH at T=80°C, P_{CO2}=0.53 bar, P_{total}=0.53 bar, NaCl=1 wt. %.

The cathodic reactions that occur on the cathode include carbonic acid, proton and water reduction. The nature and kinetics of the reactions that occur on the uncovered regions of the cathode are the same as those on the anode surface. The kinetics on the passivated cathode appear to be slower

compared with those occurring on a bare anode, probably due to the presence of an iron carbonate film. The retardation factor *f* was found to be related to the pH as depicted in Figure 5.

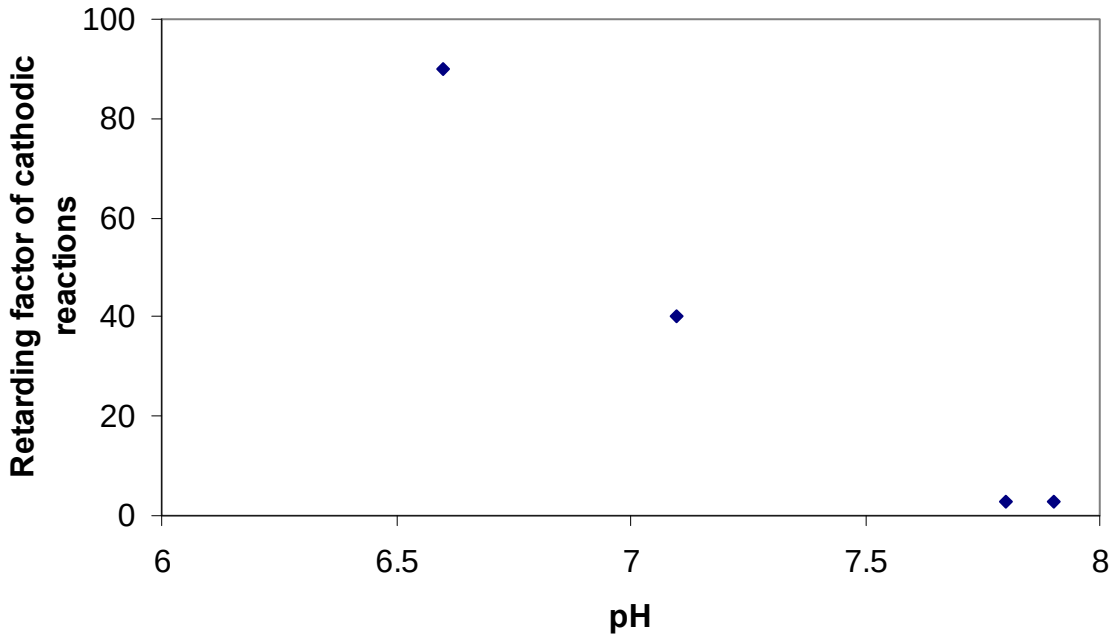

Figure 5 Retarding factor for cathodic exchange current density at T=80°C, P_{CO2}=0.53 bar, P_{total}=1 bar, NaCl=1 wt. %.

Knowing the kinetics of the anodic and cathodic reaction processes on the cathode, the open circuit potential, corrosion rate and polarization curves for spontaneous passivation on the cathode can be calculated.

Modeling the galvanic cell established between anode and cathode: The galvanic cell between anode and cathode can be modeled since the reactions on these surfaces are quantifiable. The net anodic currents from the anodic reactions on both surfaces are balanced by the net cathodic currents from the cathodic reactions on both surfaces, as shown in Figure 6. The mixed potential is the galvanic coupled potential. The current flowing between the two at the coupled potential is the galvanic current. The localized corrosion current (rate) can be calculated if the area ratio of the passivated cathode and the actively corroding pit is known. As shown schematically in Figure 6, the corrosion rate at the anode is accelerated after the galvanic cell is established.

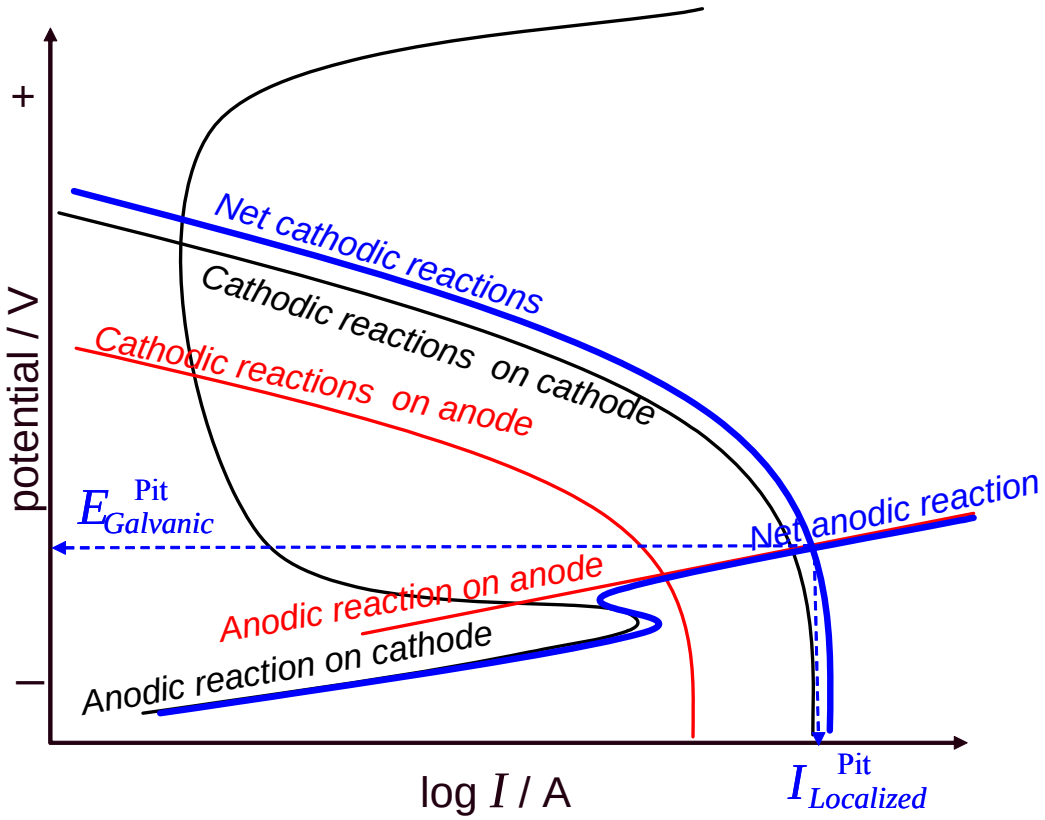

Figure 6 Schematic of the galvanic cell established between bare anode (pit) and the passive iron carbonate covered cathode.

Experimental validation of the model

The model was validated with the potentiodynamic polarization sweeps performed on a bare steel surface, passive surface and via artificial pit tests [9].

An example of a potentiodynamic polarization sweep on a bare steel surface is shown in Figure 7. Comparison of the experimental data and model prediction shows a reasonable agreement for the purposes of the present model.

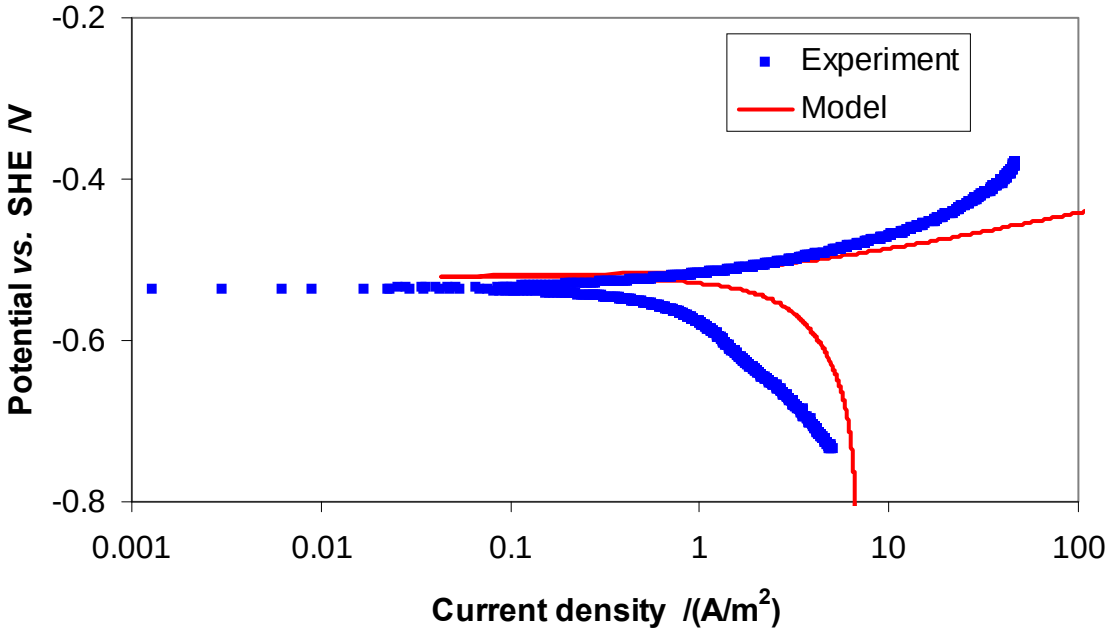

Figure 7 Model prediction matches an example of experimental polarization curves on a bare steel surface at T=80 °C, pH 7.0, P_{CO2}=0.53 bar, P_{total}=1 bar, NaCl=1 wt. %.

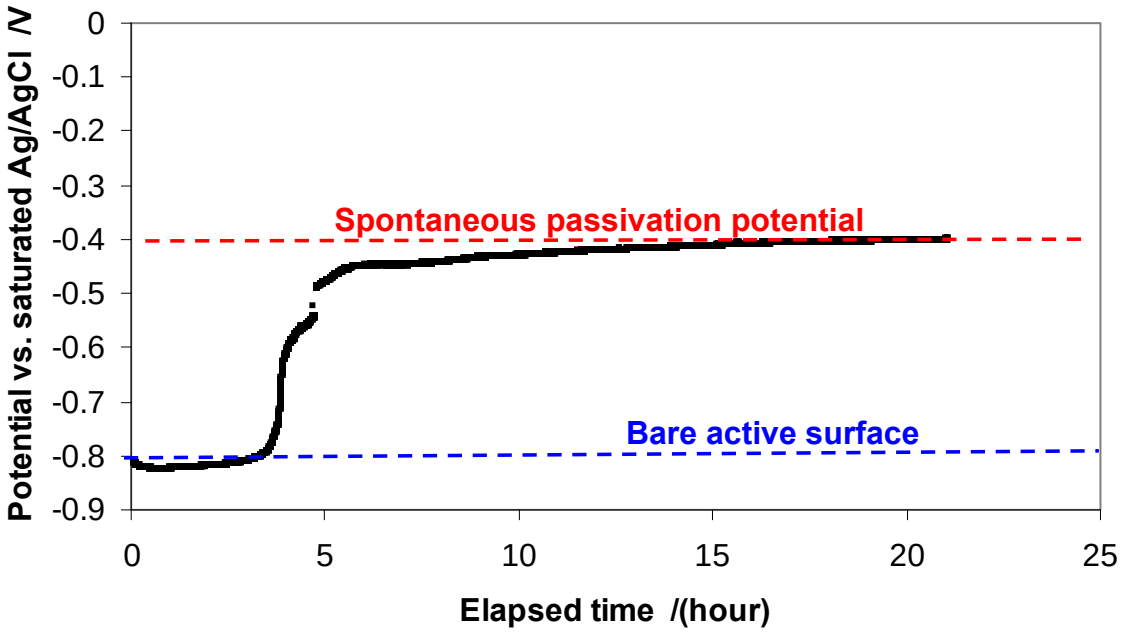

Figure 8 Open circuit potential change for the case of spontaneous passivation at T=80 °C, pH 7.8, NaCl=1 wt. %, P_{CO2}=0.53 bar, P_{total}=1 bar, $Fe^{2+}{}_i$= 0 ppm.

Figure 8 shows a typical spontaneous passivation process. At the beginning of the test, the coupon was immersed in the solution. The open circuit potential was monitored and after a while a large change in the positive direction was observed without any external applied current or potential. This is an indication of spontaneous steel surface passivation. After the surface was fully passivated, a potentiodynamic polarization sweep was conducted. Experimental results and the model prediction are compared in Figure 9, where a good agreement is observed. The predicted pH dependence of the

spontaneous passivation potential is in good agreement with the experimental data, as shown in Figure 10.

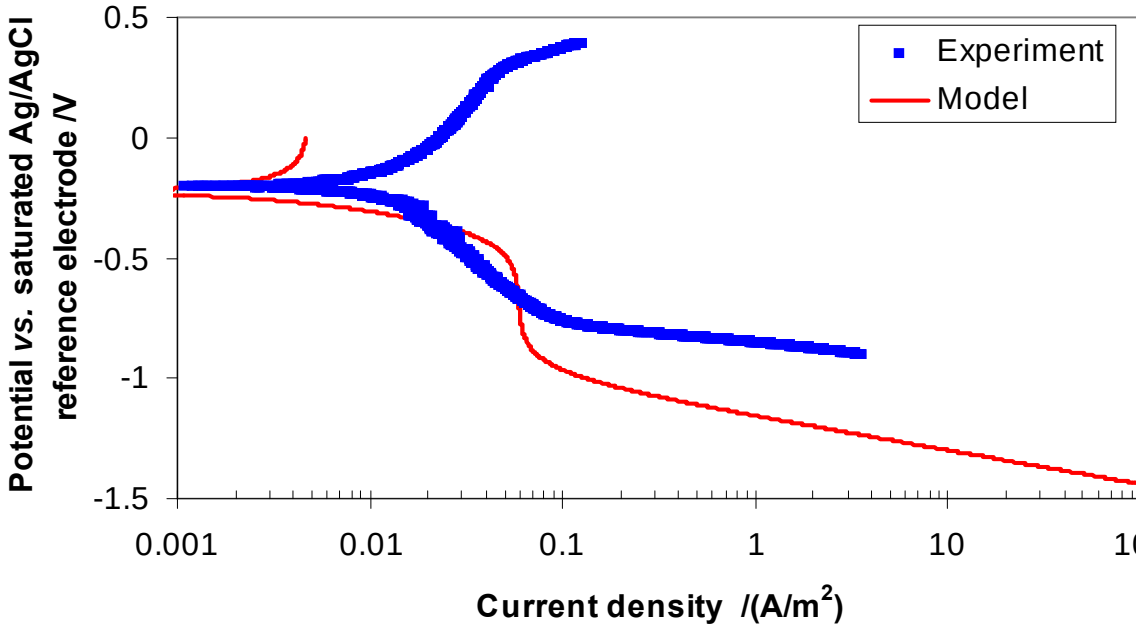

Figure 9 Comparison of model prediction and an experimental polarization curve on a passive steel surface at T=80 °C, pH 7.8, P_{CO2}=0.53 bar, P_{total}=1 bar, NaCl=1 wt. %.

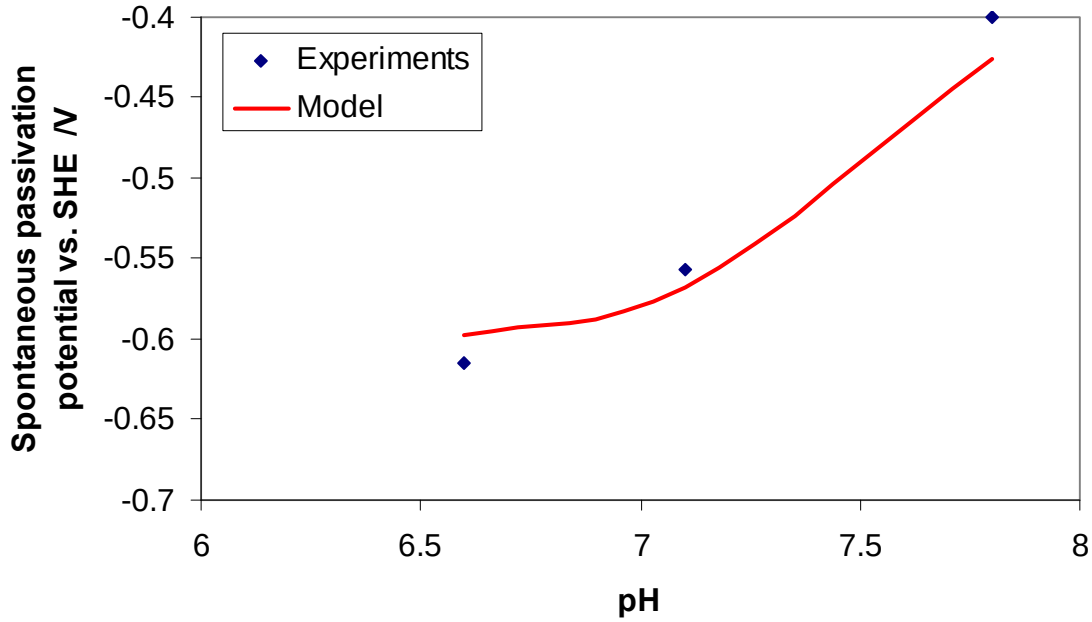

Figure 10 Comparison of a spontaneous passivation potential obtained by the model and experimental data at T=80 °C, NaCl=1 wt. %, P_{CO2}=0.53 bar, P_{total}=1 bar, $Fe^{2+}{}_i$= 0 ppm.

The galvanic cell model was validated by artificial pit tests. The set-up and procedure for the artificial pit has been previously reported [9]. The key idea behind the artificial pit test is that the cathode is initially spontaneously passivated, an example is shown in Figure 11. Subsequently a fresh small steel

anode is then introduced and serves as an anode. Its open circuit potential is lower than that of the passivated cathode surface. The two surfaces are then connected by a zero resistance ammeter (ZRA) and the resulting current measured. The data obtained are shown in Figure 12 for a cathode to anode area ratio of 350. The coupled potential lies between the open circuit potential of the active anode and passive cathode. Figure 13 focuses on the galvanic current density with respect to the anode. The experimental data shows that the galvanic current density varies within a range of 2–4 A/m^2. The prediction from the model is 7.6 A/m^2, more than twice than experimentally observed, what is considered acceptable for this early stage if the model development. A ratio of the localized corrosion rate to the uniform corrosion rate of the anode represents a measure of the severity of localized corrosion propagation. Comparison between the experimental results and model prediction for the ratio are in good agreement, as shown in Figure 14. A more detailed overview of the predictions is listed in Table 1 for this case.

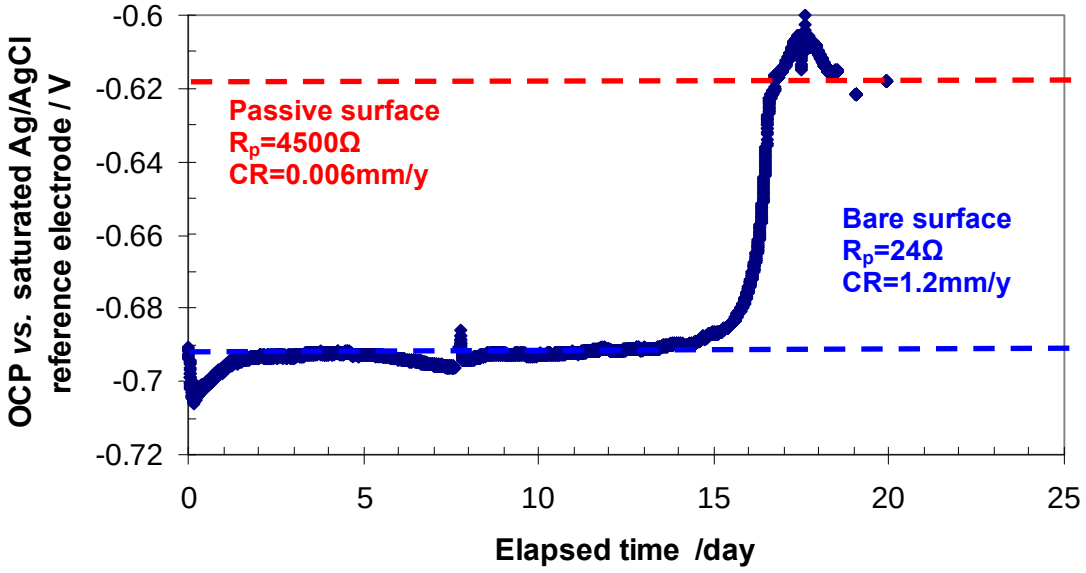

Figure 11 Open circuit potential (OCP) profile for spontaneous passivation on the cathode during the artificial pit test at T=80 °C, pH 6.6, NaCl=1 wt %, P_{CO2}=0.53 bar, P_{total}=1 bar, $Fe^{2+}{}_i$= 0 ppm.

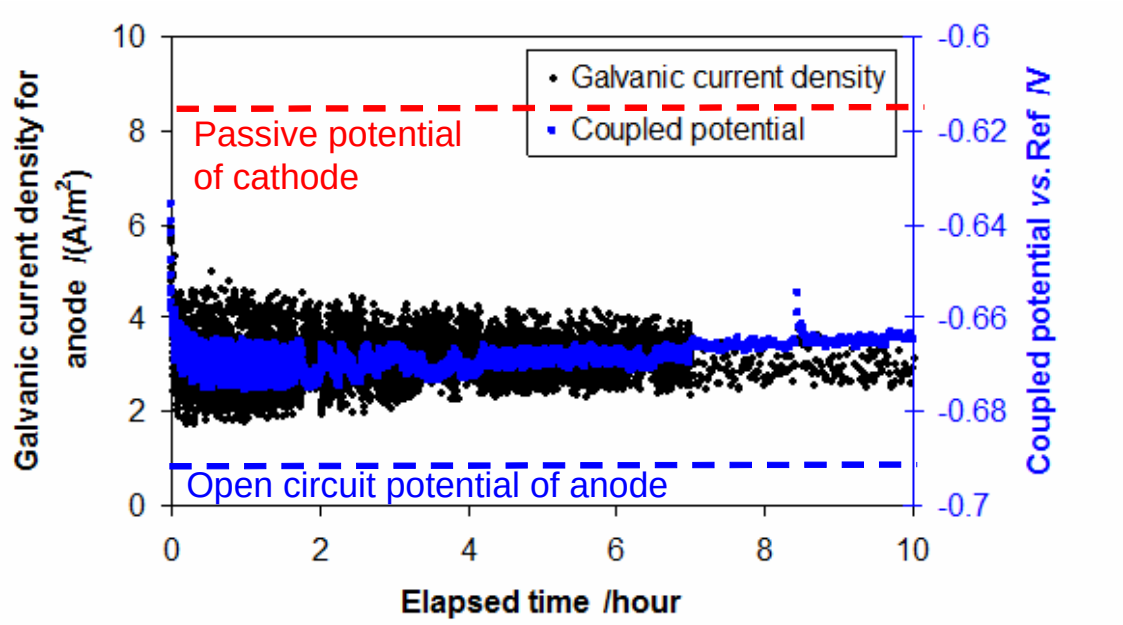

Figure 12 Galvanic current density with respect to anode and coupled potential profiles after the anode and cathode were connected during artificial pit test at T=80 °C, pH 6.6, NaCl=1 wt. %, P_{CO2}=0.53 bar, P_{total}=1 bar, $Fe^{2+}{}_i$= 0 ppm, area ratio=350.

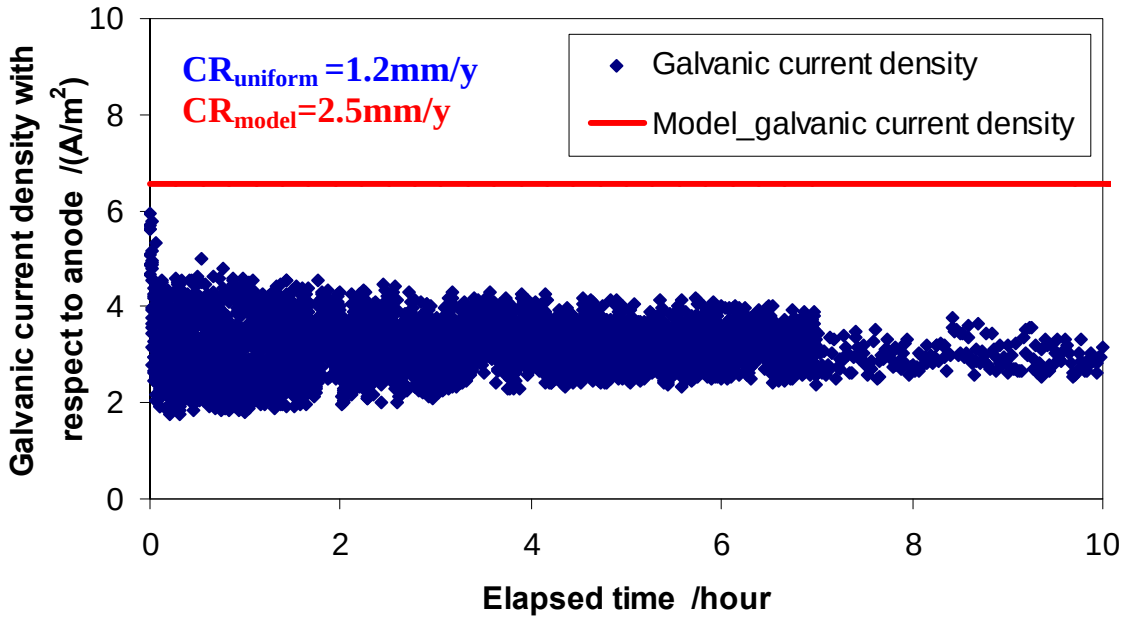

Figure 13 Galvanic current density with respect to the anode comparison between model prediction and experimental data at T=80 °C, pH 6.6, NaCl=1 wt. %, P_{CO2}=0.53 bar, P_{total}=1 bar, $Fe^{2+}{}_i$= 0 ppm, area ratio=350.

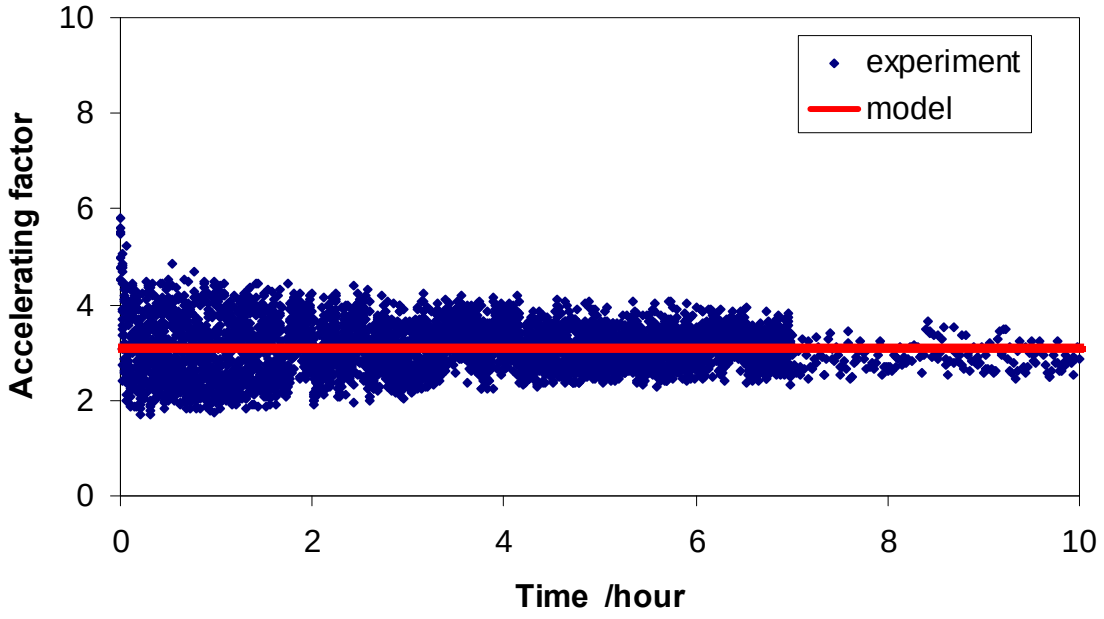

Figure 14 Predicted localized corrosion acceleration factor as a function of time; comparison between model prediction and experimental data at T=80 °C, pH 6.6, NaCl=1 wt. %, P_{CO2}=0.53 bar, P_{total}=1 bar, Fe^{2+}_i= 0 ppm, area ratio=350.

Table 1 Comparison compilation of the experimental data and model predictions

		experiment	model
OCP cathode	/ V	-0.60 to -0.62	-0.60
OCP anode	/ V	-0.69 to -0.70	-0.72
Mixed potential	/ V	-0.68 to -0.67	-0.69
Increased potential of anode	/ mV	20-30	23
CRlocalized	/(mm/y)	2.2-4.4	7.6
CRuniform	/(mm/y)	1.2	2.5
Anode accelerating factor: ($CR_{localized}/CR_{uniform}$)		1.8-3.7	3.0

Numeric tests of the model

The effects of the cathode to anode area ratio and temperature on localized corrosion rate were investigated by using the model.

Figure 15 shows the area ratio effect on localized corrosion propagation under given test conditions. The anode uniform corrosion rate is 2.5 mm/y assuming no localized corrosion. The localized corrosion rate can increase anywhere from 3 mm/y to 15 mm/y where the area ration varies from 10 to 1000.

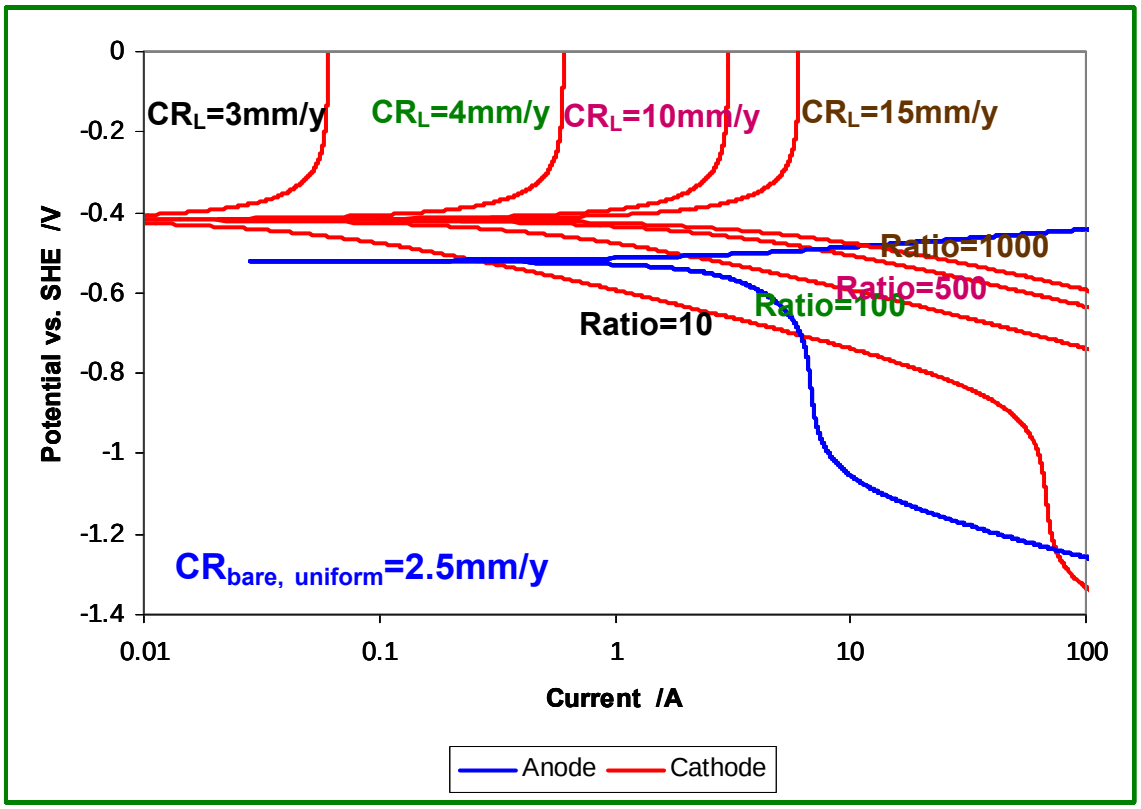

Figure 15 Model prediction for the cathode/anode area ratio effect on localized corrosion at T=80 °C, pH 7.0, NaCl=1 wt. %, P_{CO2}=0.53 bar, P_{total}=1 bar, $Fe^{2+}{}_i$= 0 ppm, $\omega_{stirring,bar}$=1000 rpm.

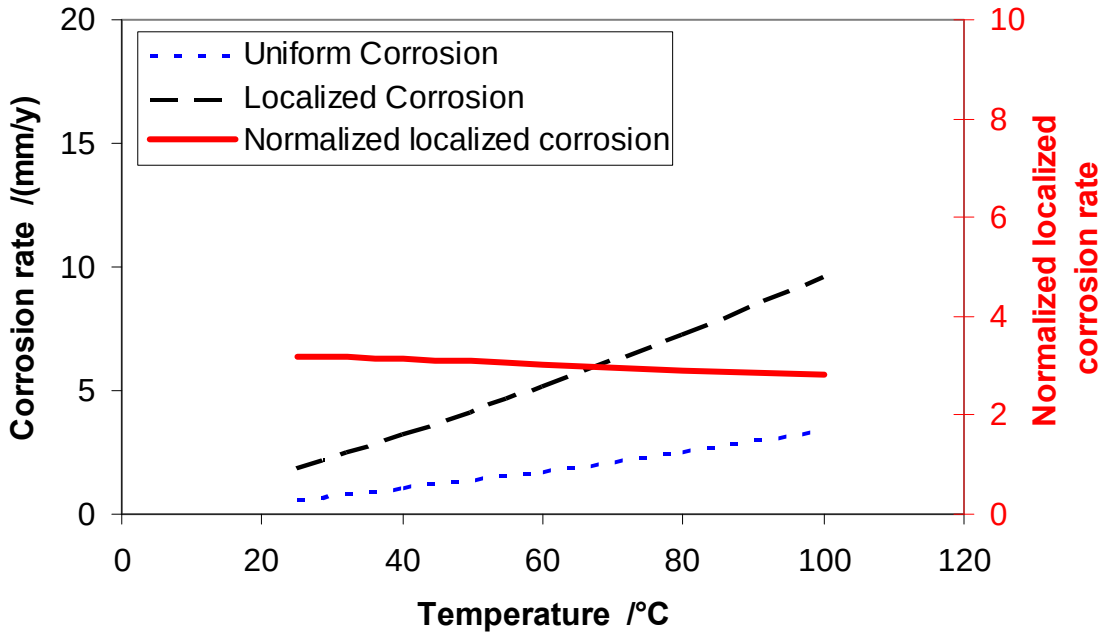

Figure 16 Model prediction for the temperature effect on localized corrosion at pH 6.5, NaCl=1 wt. %, P_{CO2}=0.53 bar, $Fe^{2+}{}_i$= 0 ppm, $\omega_{stirring,bar}$=1000 rpm, area ratio=350.

The temperature has a accelerating effect on localized corrosion propagation as shown in Figure 16. However, the uniform corrosion rate increases as well with temperature and the localized/uniform corrosion rate ratio actually decreases slightly from 4 to 3 in this temperature range. A similar effects can be seen at a different area ratio in Figure 17.

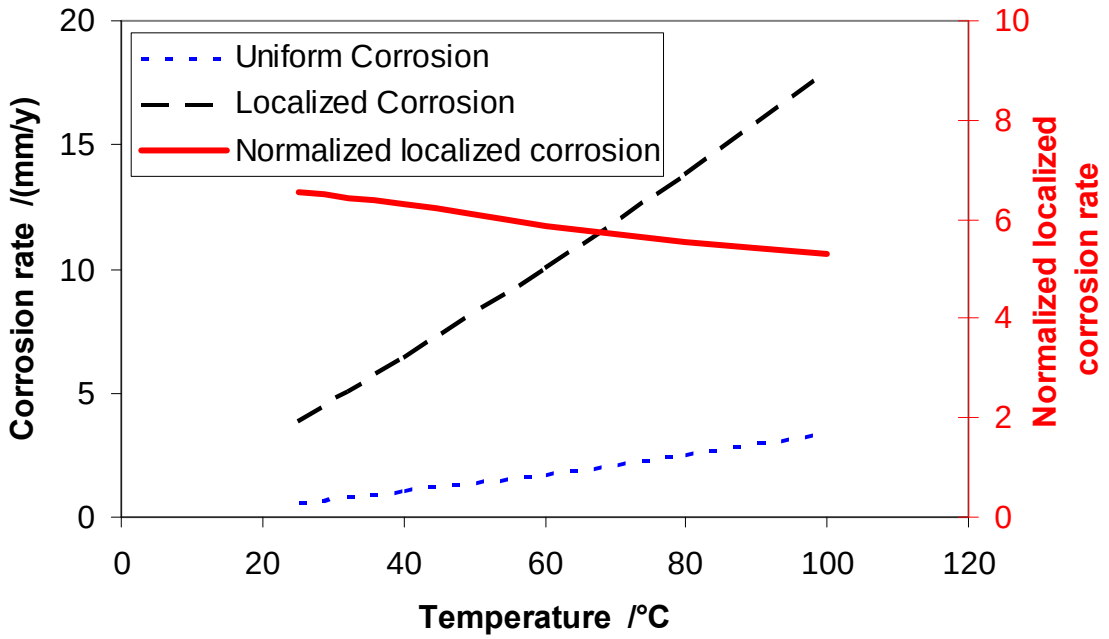

Figure 17 Model prediction for the temperature effect on localized corrosion at pH 6.5, NaCl=1 wt. %, Fe^{2+}_i= 0 ppm, $\omega_{stirring\ bar}$=1000 rpm, area ratio=1000.

CONCLUSIONS

A mechanistic electrochemical model for localized CO_2 corrosion propagation was built based on a galvanic mechanism, where it is assumed that the bare steel anode is actively corroding while the iron carbonate filmed cathode is passivated. The model is based on water chemistry, mass transfer and electrochemical calculations of the processes occurring on a bare steel anode and passivated cathode. The localized corrosion rate acceleration on the bare steel anode is a result of a galvanic current that flows between them. Electrochemical portions of the present model were validated separately by experimental data. Numerical tests demonstrate that localized corrosion propagation rates increase as the increase of the area ratio and temperature.

ACKNOWLEDGEMENTS

Helpful discussion with Dr. David Young on this paper is acknowledged. The authors acknowledge the financial support from the board company members. They are Baker Petrolite, BP, Champion Technologies, Chevron, Clariant, Columbia Gas Transmission, ConocoPhillips, Eni, ExxonMobil, MI Production Chemicals, Nalco, Occidental Oil Company, Petrobras, PTTEP, Saudi Aramco, Shell, Tenaris and Total.

REFERENCES

1. G. Schmitt, W. Bucken and R. Fanebust, Corrosion, Vol. 48, No. 5, 1991, pp. 431.

2. G. Schmitt and M. Horstemeier, "Fundamental Aspects of CO_2 metal Loss Corrosion – Part II: Influence of Different Parameters on CO_2 Corrosion Mechanism", CORROSION/2006, paper No. 06112, (Houston, TX: NACE, 1993).
3. G. Schmitt, T. Gudde and E. Strobel-Effertz, "Fracture Mechanical Properties of CO_2 Corrosion Product Scales and Their Relation to Localized Corrosion", CORROSION/96, paper No. 9, (Houston, TX: NACE, 1996).
4. G. Schmitt, C. Bosch, U. Pankoke, W. Bruckhoff and G. Siegmund, "Evaluation of Critical Flow Intensities for FILC in Sour Gas Production", CORROSION/98, paper No. 46, (Houston, TX: NACE, 1998).
5. G. Schmitt, M. Mueller, M. Papenfuss and E. Sttrobel-Effertz, "Understanding Localized CO_2 Corrosion of Mild steel from Physical Properties of Iron Carbonate Scales", NACE CORROSION/99, paper No. 38 (Houston, TX: NACE, 1999).
6. G. Schmitt, M Mueller, "Critical Wall Shear Stresses in CO_2 Corrosion of Mild steel", CORROSION/2002, paper No. 44, (Houston, TX: NACE, 1999).
7. G. Schmitt, C. Bosch, P. Plagemann and K. Moeller, "Local Wall Shear Stress Gradients in the Slug Flow Regime – Effect of Hydrocarbon and Carrosion Inhibitor", CORROSION/99, paper No. 02244, (Houston, TX: NACE, 2002).
8. M. H. Achour, J.Kolts, A. H. Johannes and G. Liu, "Mechanistic Modeling of Pit Propagation in CO_2 Environment under High Turbulence Effects", CORROSION/93, paper No. 87, (Houston, TX: NACE, 1993).
9. J. Han, Y. Yang, B. Brown and S. Nešić, "Electrochemical Investigation of Localized CO_2 Corrosion on Mild Steel". Corrosion/2007, paper No. 07323, (Houston, TX: NACE, 2007).
10. J. Han, Y. Yang, B. Brown and S. Nešić, "Roles of Passivation and Galvanic Effects in Localized CO2 Corrosion of Mild Steel", CORROSION/2008, paper No. 08332, (Houston, TX: NACE, 2008).
11. J. Han and D. Young, S. Nešić and A. Tripathi, "Characterization of the passive film on Mild Steel in CO_2 Environments", 17th International Corrosion Congress, paper No. 2511, 2008.
12. M. Nordsveen, S. Nešić, R. Nyborg and A. Stangeland, Corrosion, Vol. 59, No. 5, 2003, pp.443.
13. S. Nešić, R. Nyborg and A. Stangeland, Corrosion, Vol. 59, No. 6, 2003, pp.489.
14. S. Nešić, K-L. J. Lee, Corrosion, Vol. 59, No. 7, 2003, pp.616.